Determination of Hydroacoustic Draft Tube Parameters by High Speed Visualization during Model Testing of a Francis Turbine

Andres Müller, Sébastien Alligné, Florine Paraz, Christian Landry, and François Avellan

EPFL Laboratory for Hydraulic Machines
Avenue de Cour 33bis, 1007 Lausanne, Switzerland,
andres.mueller@epfl.ch, sebastien.alligne@epfl.ch, christian.landry@epfl.ch, francois.avellan@epfl.ch

Abstract

Francis turbines can experience critical instabilities at high load operating points, limiting their maximum power output. The swirling flow developed in the draft tube produces a cavitating axisymmetric volume, acting as an internal energy source leading to a self-excited surge phenomenon. The pulsation of the vortex rope corresponds to one of the eigenfrequencies of the hydraulic system.

Efforts to accurately characterize, simulate and predict this phenomenon have been undertaken by several researchers, using a 1-D hydroacoustic model of the full load vortex rope. The key physical parameters are the mass flow gain factor, standing for the excitation mass source of the hydraulic system, the cavitation compliance factor, representing the wave speed and the thermodynamic damping, modeling the energy dissipation between the liquid and the gas. These parameters need to be determined either numerically or experimentally. The aim of the present investigation is to determine the mass flow gain factor and the cavitation compliance using experimental data obtained during a measurement campaign on a reduced scale Francis turbine model and to compare the results to existing CFD data.

Keywords: Instability, cavitation, vortex rope, experimental measurements, hydroacoustic, full load

1. Introduction

Hydraulic power generation systems may experience critical limitations of their produced output during full load operating conditions due to flow instabilities in the draft tube cone. The self-excited oscillation of the cavitating axisymmetric vortex rope at one of the eigenfrequencies of the hydraulic system leads to high vibration and noise, preventing a further increase of power output.

Early measurements at full load on a reduced scale model presenting this type of instability were performed by Jacob et al. [8] in 1988, linking the frequency of the recorded pressure fluctuations to a computed eigenfrequency obtained by a forced excitation of the system. Studying the Pogo effect in cavitating turbo pumps, Brennen and Acosta developed in 1976 [3] and 1978 [4] a transfer function relating the pressure and the inlet flow rate fluctuations to the same quantities at the outlet, including the cavitation compliance and the mass flow gain factor as key parameters. A similar approach based on cavitation parameters mapping was used by Tsujimoto et al. in 1993 [13] to explain inducer instabilities and later by Duttweiler and Brennen in 2002 [7] and Watanabe and Brennen in 2003 [14] to explain propeller instabilities. Koutnik et al. applied the transfer matrix method to Francis turbines in 1996 [9] and performed a time domain simulation of a full load instability occurring in a Francis pumped-storage plant in 2006 [10]. Further contributions to the simulation of the full load surge were made by Chen et al. in 2007 [5], Alligné et al. in 2010 [1] and Dörfler et al. in 2010 [6], choosing different approaches modelling the physics of the draft tube flow.

The experimental determination of the parameters of the hydroacoustic model is a main challenge. This paper presents an optical method to compute the instantaneous volume of the vortex rope, necessary for the calculation of both the cavitation compliance and the mass flow gain factor. The method is based on the processing of images recorded with a high speed camera on a reduced Francis turbine model. Measuring the relevant flow parameters at four different operating points, the cavitation compliance and the mass flow gain factor are estimated.

2. Case study

The experimental data was collected in the scope of an extensive measurement campaign on a reduced Francis turbine model of specific speed $\nu = 0.27$ on the EPFL test rig PF2 in 2008. The flow in the diffuser is recorded with a high speed camera at a resolution of 1024 x 1024 pixels and an acquisition rate of 50 frames per second. The experimental setup is shown in Fig. 1. The backside of the Plexiglas cone was covered with an anti-reflective paper and the flow was being illuminated by two 800 W spotlights with linear tungsten-halogen bulbs.
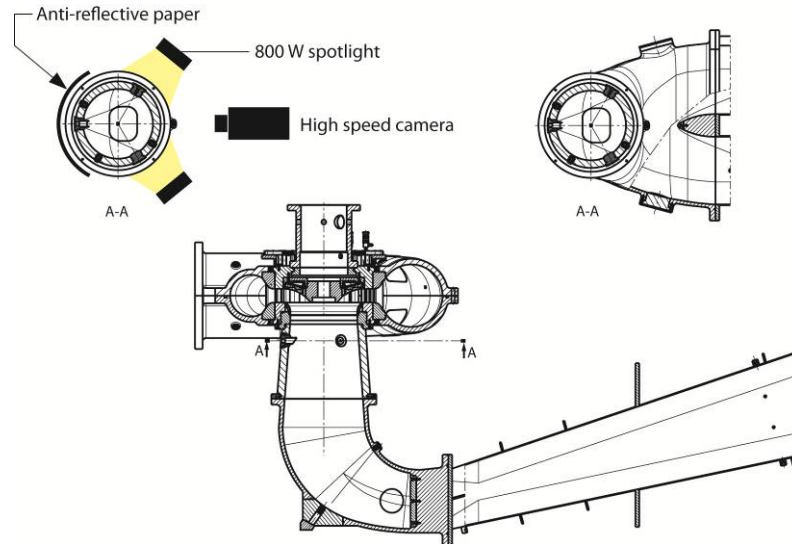
Fig. 1 Experimental setup for the measurements on the reduced model

The camera was synchronized with dynamic pressure sensors installed in the draft tube to measure the pressure fluctuations. For further details on this particular case study, please refer to [1] and [2]. A sequence of images of typical shapes of the full load vortex rope during one cycle of its volumes oscillation is shown in Fig. 2.
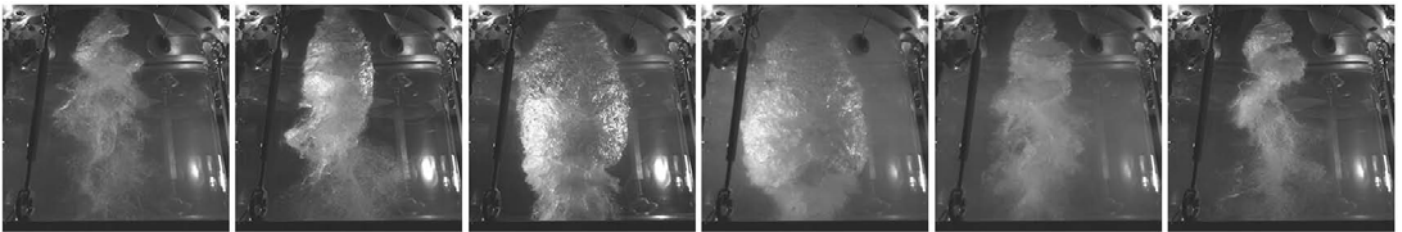
Fig. 2 Illustration of full load surge on the reduced model on EPFL test rig PF2 (OP#4)

3. Testing conditions

For the following investigation, four operating points at full load are chosen. The corresponding operating conditions are given in Table 1 for the reduced model and the existing prototype. From the nominal operating point OP#2, which possesses a Froude similitude with respect to an unstable operating point of the prototype, a variation of the Thoma number σ and Froude number Fr is performed.

Table 1 Summary of operating conditions to determine the hydroacoustic parameters χ and C_C

| Operating point number [-]	Guide vane opening [°]	E^M [J.kg^{-1}]	Q^M [m^3.s^{-1}]	N_{ED} [-]	Q_{ED} [-]	T_{ED} [-]	σ (sigma) [-]	Fr (Froude) [-]	E^P [J.kg^{-1}]	Q^P [m^3.s^{-1}]
OP#1	30.0	115.78	0.347	0.274	0.263	0.133	0.100	5.80	1786.38	324.240
OP#2	30.0	115.84	0.347	0.274	0.263	0.133	0.110	5.80	1786.80	324.015
OP#3	30.0	115.91	0.347	0.274	0.263	0.133	0.153	5.80	1787.50	324.091
OP#4	30.0	192.02	0.453	0.274	0.267	0.135	0.110	7.50	1788.77	328.75

4. Determination of the vortex rope volume

The property of vapour to reflect light, in contrast to the transparent flow of water, is used to visualize the cavitation vortex rope. The edges of the vortex rope are detected in order to deduce the volume for each frame. An important criterion of a given method is the ability to deal with problems due to inhomogeneous illumination or missing edges at certain boarder regions of the cavity. The conversion of the images to a binary format by thresholding did not produce satisfying results; therefore a second order edge detection by applying a Laplacian of Gaussian (LoG) filter was used according to [11].

The illumination of the vortex rope being not homogeneous, a brighter left part and a darker right part is identified at most stages. For the following method, the picture is split into two parts along the vertical symmetry line, treated separately and then reassembled in order to identify the edges of the cavity.

A Gaussian image smoothing recalculates the components of a (2x2) matrix, corresponding to pixel values of an image, using a normal distribution according to

$$G(x, y) = \frac{1}{2\pi\sigma^2} \exp\left(\frac{x^2 + y^2}{2\sigma^2}\right),$$

(1)

where σ is the standard deviation. The effect is a blur and the removal of details and noise from the picture. The second derivative of a Gaussian is an appropriate filter to detect intensity changes in an image and as a consequence the edges of a given object in the picture, as described by Marr and Hildreth [11]. The different steps of the image processing are shown in Fig. 3 for different stages A) - D) of the vortex rope within one cycle. The original images are shown in the top row and the results of the application of the LoG filter in the second row. The value of the standard deviation used for the Gaussian smoothing is $\sigma = 2$. The third row displays the first and the last white pixel in each horizontal line, represented by green and red crosses, respectively. It is noticed that the black and white pixels have been inverted in the second row of Fig. 3 in order to enhance the visibility on paper.
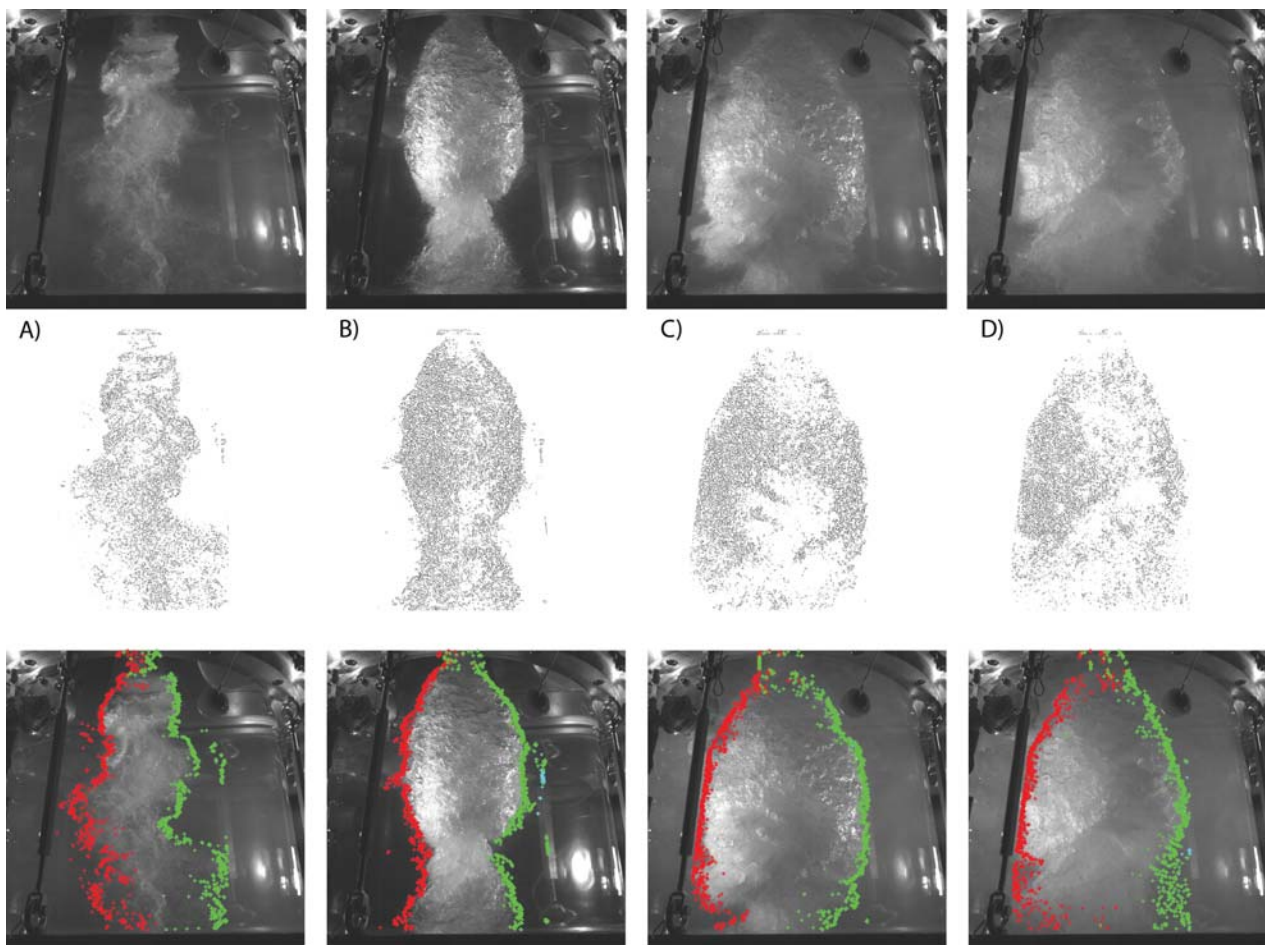
Fig. 3 Original images (top), results of LoG filtering (middle) and edges of the vortex rope (bottom) for OP#4

The volume of the vortex rope is calculated by counting the number of pixels between the red and the green cross for every horizontal plane of the image, as illustrated at the bottom of Fig. 3. Knowing the geometry of the cone, this number can be converted to an equivalent diameter of the assumed axisymmetric vortex rope at a given location and the different cross sections are then added up to an approximate volume; the inclination angle of the camera; not being taken into account. The dimensionless time dependant fluctuation of the vortex rope volume is shown in Fig. 4 for OP#4. The volume is divided by the total volume of the Plexiglas cone and the time is made non dimensional by the rotating speed of the runner n. The oscillation is periodical at a frequency of 0.17 times n.
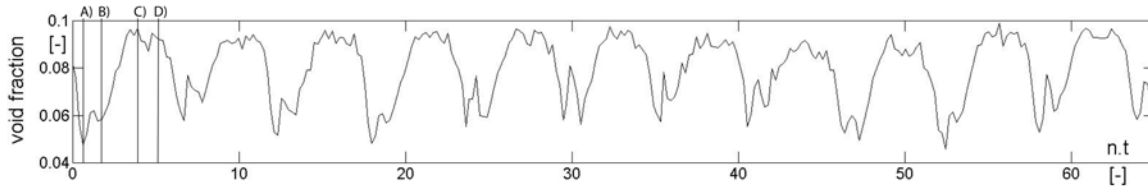

Fig. 4 Vortex rope volume as a function of time for the operating point OP#4

For the determination of the hydroacoustic parameters, a mean value of the cavity volume is calculated. This value is given in Table 2, together with the dimensionless flow parameters and the discharge for the investigated operating points. The mean vortex rope volume as a function of the Thoma number and the discharge, respectively, is shown in Fig. 5 including the standard deviation at each operating point.

Table 2 Mean vortex rope volume for different operating points

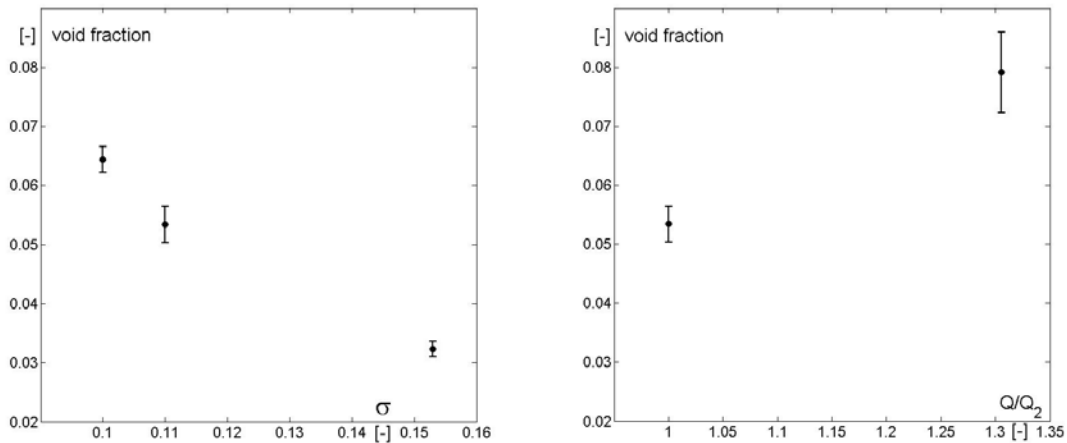| Operating point number [-]	Q^M [m³.s⁻¹]	σ (sigma) [-]	Fr (Froude) [-]	Mean volume [m³]	Number of images [-]
OP#1	0.347	0.100	5.80	0.0028751	201
OP#2	0.347	0.110	5.80	0.0023842	301
OP#3	0.347	0.153	5.80	0.0014431	301
OP#4	0.453	0.110	7.50	0.0035331	301

Fig. 5 Mean volume as a function of the Thoma number (left) and the discharge (right)

5. Calculation of the hydroacoustic parameters

A new 1-D model for the draft tube was developed by Alligné et al. [2] for an accurate stability analysis with the in-house software SIMSEN. The model is shown in Fig. 6, featuring the mass flow gain factor χ, representing the effects of the swirling flow in the diffuser, the cavitation compliance C_C, standing for the compressibility of the gaseous volume and a damping coefficient R_{ve}, taking into account the thermodynamic exchange between liquid and gas.
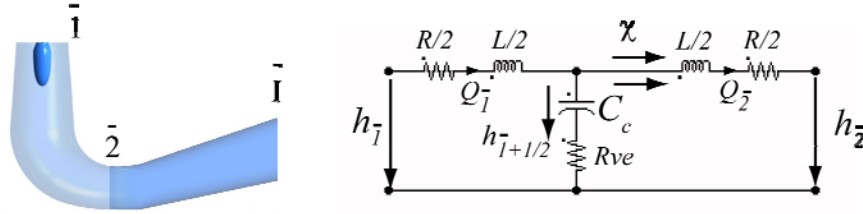
Fig. 6 Draft tube domain (left) and equivalent electrical scheme of the set of cone and elbow parts (right) [1]

The node equation in the electrical scheme corresponds to the continuity equation between the runner outlet $\left(\overline{1}\right)$ and the elbow outlet $\left(\overline{2}\right)$:

$$Q_{\overline{1}} - Q_{\overline{2}} = \frac{DV_C}{Dt} = C_C \frac{dh_{\overline{1}+1/2}}{dt} + \chi \frac{dQ_{\overline{2}}}{dt} \tag{2}$$

$Q_{\overline{1}}$ represents the discharge at the runner outlet, $Q_{\overline{2}}$ the discharge at $A_{\overline{2}}$, $h_{\overline{1}+1/2}$ the piezometric head at the node in-between and V_C the vortex rope volume. The cavitation compliance C_C and the mass flow gain factor χ are hence defined as

$$C_C = -\frac{\partial V_C}{\partial h_{\overline{1}+1/2}} \quad \text{and} \quad \chi = -\frac{\partial V_C}{\partial Q_{\overline{2}}}. \tag{3}$$

Cavitation compliance factor C_C

The cavitation compliance can also be expressed as a function of the Thoma number, assuming

$$C_C = -\frac{\partial V_C}{\partial h_{\overline{1}+1/2}} \approx -\frac{\partial V_C}{\partial h_{\overline{1}}} = -\frac{1}{H}\frac{\partial V_C}{\partial \sigma}. \tag{4}$$

The necessary values are obtained by comparing the change in the vortex rope volume V_C and in the Thoma number σ for the operating points OP#1 and OP#3. Using the values in Table 1 and Table 2, the cavitation compliance becomes

$$C_C \approx -\frac{1}{H}\frac{\Delta V_C}{\Delta \sigma} = 228.8 \cdot 10^{-5} \pm 6.3 \cdot 10^{-5} \text{ m}^2, \tag{5}$$

where the uncertainty interval is obtained by computing the cavitation compliance using the maximum and the minimum values of the volumes V_C. The compliance can also be written as a function of the speed of sound [12], as in

$$C_C = -\frac{\partial V_C}{\partial h_{\overline{1}+1/2}} = \frac{g \cdot A \cdot l}{a^2}. \tag{6}$$

Using eq. (5) in eq. (6) finally yields

$$a = \sqrt{\frac{g \cdot A \cdot l}{C_C}} = 28.0 \pm 0.4 \text{ m} \cdot \text{s}^{-1}. \tag{7}$$

Mass flow gain factor χ

For the calculation of the mass flow gain factor, the changes in the vortex rope volume and the discharge between the operating points OP#2 and OP#4 are considered and used in

$$\chi = -\frac{\partial V_C}{\partial Q_{\bar{2}}} \approx -\frac{\Delta V_C}{\Delta Q_{\bar{2}}}. \tag{8}$$

Given the values in Table 1 and Table 2, the mass flow gain factor becomes

$$\chi \approx -\frac{\Delta V_C}{\Delta Q_{\bar{2}}} = -10.8 \cdot 10^{-3} \pm 1.6 \cdot 10^{-3} \ \ \text{s}. \tag{9}$$

The calculated values for the cavitation compliance and the mass flow gain factor are compared to numerical results obtained with CFD by Alligné et al. [1], [2] and are found to lie within the same order of magnitude.

6. Conclusions

The cavitation compliance and the mass flow gain factor play an important role in predicting the stability of hydraulic systems using a hydroacoustic 1-D model. These two key parameters were calculated based on a high speed visualization of the cavitation vortex rope. A tool to determine the instantaneous volume of the vortex rope processing the images from a high speed camera was developed. The applied Laplacian of Gaussian filter detects accurately the edges of the vortex rope, despite the inhomogeneous illumination of the cavity.

Acknowledgments

Nomenclature

A	Pipe cone section area [m^2]	L	Inductance [s^2.m^{-2}]
a	Wave speed [m.s^{-1}]	n	Runner rotational frequency [s^{-1}]
C	Electrical capacitance [m^2]	N_{ED}	Speed factor [-]
C_C	Cavitation compliance [m^2]	Q	Volumetric discharge [m^3.s^{-1}]
E	Machine specific energy [J.kg^{-1}]	Q_{ED}	Discharge factor [-]
Fr	Froude number [-]	R	Electrical resistance [s.m^{-2}]
g	Gravitational acceleration [m.s^{-2}]	R_{ve}	Thermodynamic resistance [s.m^{-2}]
h	Piezometric head [m]	t	Time [s]
H	Hydraulic head [m]	V_C	Cavity volume [m^3]
l	Length of cone and elbow parts [m]	χ	Mass flow gain factor [s]

References

[1] Alligné, S., 2011, "Forced and Self-oscillations of Hydraulic Systems induced by Cavitation Vortex Rope of Francis Turbines", Ph. D. Thesis No. 5117, Ecole Polytechnique Fédérale de Lausanne, Switzerland

[2] Alligné, S., Maruzewski, P., Dinh, T., Wang, B., Fedorov, A., Iosfin, J. and Avellan, F., 2010, "Prediction of a Francis turbine prototype full load instability from investigations on a reduced scale model", 25th IAHR Symposium on hydraulic Machinery and Systems, Timisoara, Romania

[3] Brennen, C. and Acosta, A., 1976, "The dynamic transfer function for a cavitating inducer", Journal of Fluids Engineering, No. 98, pp. 182-191.

[4] Brennen, C., 1978, "Bubbly flow model for the dynamic characteristics of cavitating pumps", Journal of Fluid Mechanics, No. 89, pp. 223-240.

[5] Chen, C., Nicolet, C., Yonezawa, K., Farhat, M., Avellan, F. and Tsujimoto, Y., 2008, "One dimensional analysis of full load draft tube surge", Journal of Fluid Engineering, No. 130, pp. 041106-1 - 041106-6.

[6] Dörfler, P., Keller, M. and Braun, O., 2010, "Francis full-load surge mechanism identified by unsteady 2-phase CFD", 25th IAHR Symposium on hydraulic Machinery and Systems, Timisoara, Romania.

[7] Duttweiler, M. and Brennen, C., 2002, "Surge instability on a cavitating propeller", Journal of Fluid Mechanics, No. 458, pp. 133-152

[8] Jacob, T., Prénat, J.-E. and Maria, D., 1988, "Comportement dynamique d'une turbine Francis à forte charge. Comparaisons modèle-prototype", La Houille Blanche, No. 3/4, pp. 293-300.

[9] Koutnik, J., Pulpitel, L., 1996, "Modelling of the Francis turbine full load surge", IAHR Symposium on Hydraulic Machinery and Systems, Lausanne, Switzerland

[10] Koutnik, J., Nicolet, C., Schohl, G. and Avellan, F., 2006, "Overload surge event in a pumped-storage power plant", Proceedings of the 23rd IAHR Symposium on Hydraulic Machinery and Systems, Yokohama, Japan

[11] Marr, D. and Hildreth, E, 1979, "Theory of edge detection", Proceedings of the Royal Society, No. 207, pp. 187-217

[12] Nicolet, C., 2007, "Hydroacoustic modelling and numerical simulation of unsteady operation of hydroelectric system", Ph. D. Thesis No. 3751, Ecole Polytechnique Fédérale de Lausanne, Switzerland

[13] Tsujimoto, Y., Kamijo, K. and Yoshida, Y., 1993, "A theoretical analysis of rotating cavitation in inducers", Journal of Fluids Engineering, No. 115, pp. 135-141

[14] Watanabe, S. and Brennen, C., 2003, "Dynamics of a cavitating propeller in a water tunnel", Journal of fluids engineering, No. 125, pp. 283-292